Responses to the reviewer's comments

We sincerely thank the reviewer for providing valuable comments to improve the manuscript. We have revised the manuscript in accordance with your comments and suggestions and provided additional information and interpretation.

1. R is usually referred to as (spectral) irradiance reflectance or, alternatively, irradiance ratio. The term "diffuse" reflectance (also in the title) suggests that direct parts of the downwelling irradiance are not taken into account. Consult the oceanopticsbook.info for widely used terminology.

It is understood that R can be referred to as the diffuse reflectance when it is evaluated just beneath the water (sea or lake) surface. Since the present work focuses on R at depths, the more correct expression for R is "Irradiance reflectance" or "Subsurface reflectance" as already noted in our earlier paper. Hence, the "diffuse reflectance" term is replaced by "Irradiance reflectance" to follow exact physics.

2. The definition of R should appear in the abstract.

Definition of R has been added to the abstract as follows, "Irradiance reflectance (*R*) is the ratio of the upwelling to the downwelling irradiances that can be related to the Gordon's parameter $(b_b/(a+b_b))$ through a proportionality factor '*f*'."

3. Abstract: "The model is valid for a wide range waters within coastal and open-ocean environments." And inland waters – as the title suggests – too?

In the revised manuscript, the sentence is rephrased as:
"The model is applicable for both marine and inland waters." Here inland water refers to lagoons within coastal environments.

4. Page 1894, 26: R is a measure of how much of the radiance travelling in all downward directions is reflected upward into any direction. The definition provided here is not clear. Also, if R varies between 0 and 1, how can it beyond 1?

Definition of *R* is elaborately described and it has been included in the revised manuscript. In fact, various fields have their own terminology for reflectance. . Reflectance in its basic physical term is defined as the ratio of the incoming and outgoing radiant fluxes and thus it has no unit. It varies between 0 to 1, whereby 0 corresponds to complete transmission and 1 to complete reflection. The reflectance values sometimes go beyond 1 for strongly forward reflecting surfaces such as snow (Painter & Dozier., 2004; Schaepman-Strub et al., 2006). In oceanography, unlike used in other fields, the measured *R* is not from an ideal diffuse reflector (Lambertian) nor the incident lighting is isotropic. Thus, it is proper to denote this quantity as "irradiance reflectance" rather than "diffuse reflectance".

An additional reference has been added to the reference list.

Painter, T. H. and Dozier, J.: Measurements of the hemispherical-directional reflectance of snow at fine spectral and angular resolution, J. Geophys. Res., 109(D18), D18115, doi:10.1029/2003JD004458, 2004.

5. Page 1895, 28 ff: The innovation of the article or model is not totally clear to me.
Differences to the previous model must be clearly highlighted and justified by means of validation to show the improved performance. To include measured IOPs does not automatically mean that the model is more accurate. This has to be proven by careful inter-comparison.

The aim of the present model has been explained concisely as follows, "The drawbacks of the existing models that were developed based on radiative transfer simulations are overcome by this model, which is solely dependent on the IOPs and illumination conditions. The objective of the present study is to propose an alternate model without involving any constants and assumptions for predicting the irradiance reflectance in a wide range of marine and inland waters. The irradiance ratio just below the surface ($R(0^-,\lambda)$) and at different depths ($R(\lambda,z)$) is modelled through the function f predicted for just below the surface ($f(0^-,\lambda)$) and at different depths ($f(\lambda,z)$) without relying on any assumptions and wavelength-dependent constant".

Difference between the previous model: Inter-comparison is included:
Comparing with the existing models, it should be noted that the existing models are designed with certain assumptions to predict *R* in case 1 waters or coastal (case 2) waters. For instance, a model that is originally developed for clear oceanic case 1 waters (Gordon et al., 1975; Morel and Prieur, 1977, Kirk, 1984) gives biased reflectance values in turbid coastal and productive water types. A model of case 2 waters (Albert and Mobley, 2003) is restricted to case 2 waters (Dev and Shanmugam, 2014b). Thus, it is more appropriate to compare the results of this study with our previous model since both the models are designed for both marine and inland waters. Figure 5(a)-(d) shows the scatter plots comparing the model *R* (from the model of Dev and Shanmugam (2014b) and this study) with *in-situ R* for all the water types, where the blue dots represent the previous model (Dev and Shanmugam, 2014b, denoted as *DS* in Table 3) and the orange dots represent the present model (denoted as *PM* in Table 3) for the key wavelengths 412, 443, 488, 531, 555, 650, 685, 715nm. In Fig. 5(a), results from both the models are nearly identical although the previous model slightly performs better (relative error 18.8%) than the present model (relative error 21.3%). These differences are noticeable in the range below 0.001 where the instrument noise could cause errors in clear oceanic waters when the reflectance values are almost zero in the NIR. In type II relatively clear waters, results from the present model start improving upon those of the previous model (Figure 5(b)), with the relative error of 18.2% for the present model and 15.3% for the previous model. The present model gives better results for the moderately turbid type III waters than the previous model (see the orange dots falling on the 1:1 line in Figure 5(c)). The relative error percentage of the present model is 10.5% when compared to 12.8% for the previous model. In Type IV sediment dominated turbid waters (Figure 5(d)), the present model yields the error percentage of <6% whereas the previous model yields around 21.3%. In the turbid productive type V waters, results from the present model are closer to the *in-situ* data (Figure 5(e)), thereby yielding the relative percentage error of less than 9% over 48% for the previous model. These results suggest that the model is well suited for optically complex coastal and inland waters with high organic and inorganic contents. These validation results clearly emphasize the importance of the present model for predicting *R* in a

wide variety of waters without involving the spectral constants with the previous model. The additional parameters with the present model increase its potential and wider applicability.

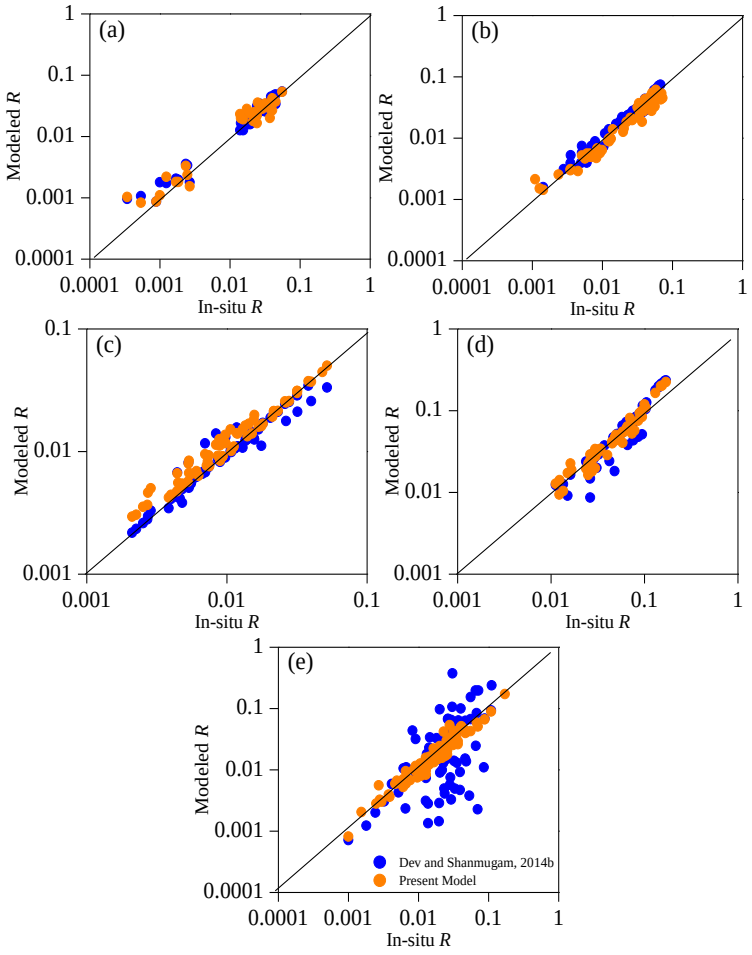

Figure 5. Scatter plots comparing the present model *R*, previous model and in-situ *R* for **(a)** type I, **(b)** type II, **(c)** type III, **(d)** type IV and **(e)** type V respectively. (Blue dots represent Dev and Shanmugam (2014b) and orange dots represent present model).

6. In the end, it is still not clear to me how the model works. What exactly are the input parameters; IOPs (absorption and backscattering coefficients) with sun zenith angle (introduce the parameter theta_s!) and chlorophyll concentration? Are the coefficients spectrally or at 400 nm only?

The following text has been included in the revised manuscript.
The calculation of $R(0^-,\lambda)$ requires four inputs namely *Chl* concentration, spectral absorption and backscattering coefficients and solar zenith angle. $R(\lambda,z)$ requires as input the $R(0^-,\lambda)$ (calculated from above four inputs) and vertical diffuse attenuation coefficients $K_u(\lambda,z)$ and $K_d(\lambda,z)$.

The backscattering and absorption denoted with 0^- represent the surface measurements and λ the spectral function. The $a(412)$ in I_f is the surface measured absorption coefficient at 412nm.

7. How is Kd and Ku determined and defined in this work?
The following formula has been included in the revised manuscript.

The Ku and Kd can be defined as,

$$K_{u,d}(\lambda, z_1 \leftrightarrow z_2) = \left(\frac{1}{z_2 - z_1}\right)\left[\ln\left(\frac{E_{u,d}(z_1)}{E_{u,d}(z_2)}\right)\right]$$

8. The attenuation coefficient, which is measured with an AC-S, the backscattering coefficient, which is measured with a BB-9 (at nine channels), and chlorophyll concentration, measured with FLNTU based on – as I think – insufficiently understood fluorescence, have – as I think – a very high uncertainty level. For example, it has become clear that in situ absorption measurements using the AC-S are subject to significant potential errors associated with imperfect correction for scattering artifacts (McKee, D., Piskozub, J., & Brown, I. (2008). Scattering error corrections for in situ absorption and attenuation measurements. Optics express, 16(24), 19480-19492.). A discussion section should be devoted to the summation of uncertainties from each model input parameter. How sensitive is the model to input changes.

The AC-S measured attenuation and absorption coefficients are corrected for temperature and salinity dependencies using the procedure recommended by Sullivan et al. (2006). For scattering error correction on the salinity-temperature corrected attenuation and absorption coefficients, Zaneveld et al. (1994) method was followed.

We understand that scattering error correction by McKee et al (2008) may be better than the Zaneveld et al. (1994) method applied in this study. The new procedure by McKee et al (2008) involves more inputs like b_{bp} and follows a complex iterative procedure. Our claim is that the abnormal values in $f(0^-,\lambda)$ (as seen through S_f, I_f & $(bb/a)^n$) (Figure 2) are not due to the imperfect correction method but due to the unaccounted inelastic processes by the photometers.

A separate description has been added to the revised manuscript as follows, "Conversely, the term 'backscattering by absorption ratio' (b_b/a) gives the spectral character to $f(0^-,\lambda)$. The spectral slope is governed by the parameter 'n', a function of *Chl* [Fig. 2(d)] (Okami et al., 1982). In case of clear oceanic waters, the spectral slope 'n' is small and thereby produces almost linear $f(0^-,\lambda)$. This is the reason why the case 1 models assume $f(0^-,\lambda)$ as a constant. For productive waters with elevated C*hl* concentrations, the slope causes large spectral variations in $f(0^-,\lambda)$ [Eq. 6]. For clear waters (assuming *Chl* = 0.1 mg m^{-3}), it takes the value of 0.194, and for turbid productive waters (*Chl* = 72 mg m^{-3}), it takes the value of 0.28. The $(b_b/a)^n$ on $f(0^-,\lambda)$ (Eq. 5) is significant due to the combined effect of absorption, fluorescence and backscattering of phytoplankton in the red and NIR regions, particularly at elevated concentrations in productive waters. The high chlorophyll effect is thus accounted in $f(0^-,\lambda)$".

Here two additional references have been added to the reference list.

Sullivan, J. M., Twardowski, M. S., Zaneveld, J. R. V, Moore, C. M., Barnard, A. H., Donaghay, P. L. and Rhoades, B.: Hyperspectral temperature and salt dependencies of absorption by water and heavy water in the 400-750 nm spectral range., Appl. Opt., 45(21), 5294–309, 2006.

Zaneveld, J. R. V., Kitchen, J. C. and Moore, C.: Scattering error correction of reflecting-tube absorption meters, in Ocean Optics XII, vol. 26, pp. 44–55, International society for Optics and Photonics, 1994.

9. Page 1899, 3 ff: I don't really understand why the absorption coefficient at 400 nm is chosen. The mentioned dominance of pure water absorption starts – in the presence of phytoplankton – rather beyond 500 or 600 nm, depending on the concentration. The 400 nm spectral range is strongly affected if CDOM (and also mineral absorption) is present. From a remote sensing point of view, this spectral range would be a rather bad choice because of critical aerosol-depending atmospheric correction. Please specify your selection.

The selection of the wavelength of 400nm is revised to 412nm. The I_f part of the model equation is changed as follows

$$I_f = 0.0684 * \left(\frac{1}{a(400)} \right)^{0.757}$$ (former I_f)

$$I_f = 0.0671 * \left(\frac{1}{a(412)} \right)^{0.756}$$ (new I_f) (included in the revised manuscript)

Due to the change of wavelength from 400nm to 412nm, the coefficients got slightly changed from 0.0684 to 0.0671 (in magnitude) and 0.757 to 0.756 (in the power). We decided to shift the wavelength from 400 to 412nm because latter one (412nm) has direct applications to remote sensing as most of the ocean color sensors realize its potential applications. Since the present model corresponds to the reflectance (which contain the information of phytoplankton, mineral particles, detritus and CDOM), choosing a wavelength in the lower blue end can give more accurate rather than choosing on the higher wavelength parts particularly>500nm, where pure water absorption dominates. Differences between the constituents (phytoplankton, mineral particles, detritus, CDOM) are more easily predicted and differentiated in the region <443nm. Thus, we have used 412 as an appropriate wavelength.

The difference between the coefficients are small when derived from a(400) and a(412). When I_f is calculated based on the new absorption wavelength 412, I_f improves slightly by <3 percent.

Type I I_f drops by 0.02307 (2.3%), Type II I_f drops by 0.00307 (0.3%), Type III I_f drops by 0.014 (1.4%), Type IV I_f improves by 0.031 (3.1%) and Type V I_f improves by 0.0303 (3.03%).

In the overall calculation of R, the plotted parameterization and spectral graphs do not seem to show any change visually, but the changes are observed in decimals ~0.0005 (0.05%).

The new coefficients are added to the Eq. 5 in the manuscript and the corresponding parameterization plot in Figure 2(c) also has been replaced.

10. Page 1900, 1 ff: The irradiance ratio, R, is probably not equal throughout the water column; near the surface it might differ because of total reflection of upwelling radiation and thus additional downwelling radiance contribution. However, it's quite homogeneous a bit deeper. Fluctuations of R in the water column are also associated with possible insufficient averaging of downwelling irradiance measurements, which exhibit large variability due to wind-related light fluctuations in the upper layer. This is why the measurement method of R should be mentioned and carefully discussed. In the corresponding Figure 4 necessary information on water depth, wind speed, and stratification of IOPs are missing. If the depth is 6 to 10 m only (near shore), we could assume strong vertical mixing of the whole water body due to waves and thus rather well mixed water?

Detailed explanation has been added to the revised manuscript as follows, "The model consistency to predict the vertical profiles of reflectance is further investigated. Figure 4(a-c) displays the variation of R throughout the water column. For brevity, the results are shown only for three different cases that vary vertically due to the IOPs. AOP profile measurements $E_u(\lambda,z)$ and $E_d(\lambda,z)$ may contain possible errors in the near surface (due to the wind-wave action / light focusing / instrument tilt) that it might suffer because of total reflection of upwelling radiation and thus the additional radiance contribution to the downwelling part. To minimize the possible errors due to the wave effects, generally the averaging of AOP/IOP measurements is done throughout the water column. Here, we evaluated the irradiance ratio $R(\lambda,z)$ through Hydrolight simulations to ignore the effects caused by the wind. Depth profiles of chlorophyll and IOPs such as a, c and b_b obtained from field measurements were given as inputs (three cases are shown in Fig. 4) and the corresponding irradiance profiles were generated for given wind speed and solar angles. $R(\lambda,z)$ was calculated from the irradiance ratio $E_u(\lambda,z)/E_d(\lambda,z)$ and the vertical diffuse attenuation coefficient (Eq. 10, these parameters are required for Eq. 7 to predict $R(\lambda,z)$).

$$K_{u,d}(\lambda, z_1 \leftrightarrow z_2) = \left(\frac{1}{z_2 - z_1}\right)\left[\ln\left(\frac{E_{u,d}(z_1)}{E_{u,d}(z_2)}\right)\right] \qquad (10)$$

Hydrolight simulations of $R(\lambda,z)$ showed that it obeys the model equation (Eq. 2) and confirms the vertically increasing/decreasing trends in the water column. Note that since the water constituents are not homogeneously distributed with depth, R cannot be constant throughout the water column and can either increase or decrease vertically depending on the constituents present in it (Hirata, 2003; Fig 16 in Sundarabalan and Shanmugam (2015)). Fluctuations in $R(\lambda,z)$ can be accurately predicted by the exponential term 'K_u-K_d' in Eqs. 2 and 7. For example, if $K_u > K_d$, R decreases; if $K_u < K_d$, R increases; or if $K_u/K_d > 1$, R decreases; if $K_u/K_d < 1$, R increases. The value of the diffuse attenuation ratio K_u/K_d, gives the proportionate increase/decrease of R with respect to the reflectance on the layer above. Though K_u and K_d can be derived from IOPs, the present model uses K_u and K_d values from calculated using Eq. 10. Assuming K_u and K_d as a sole function of IOPs ($K_u \sim K_d \sim a+b_b$) would rather lead to a constant R throughout the depth, which is not practically applicable in cases other than homogeneous waters. Thus, the present model of $R(z)$ requires $R(0^-,\lambda)$ (calculated purely from IOPs and incident sun angle) and vertical diffuse attenuation coefficients K_u and K_d.

The Hydrolight input and output profiles for three different stations (row wise) are plotted in Figure. 4(a–c). For brevity the depth profiles of green wavelength are only shown. The depth profiles of *Chl*, *turbidity*, total *a*, total *c* and total b_b are the inputs and $E_u(\lambda,z)$, $E_d(\lambda,z)$ are the outputs for given wind speed and solar zenith angles. $K_u(\lambda,z)$, $K_d(\lambda,z)$ and $R(\lambda,z)$ are calculated as discussed above. The non-homogeneous IOP profiles are selected to show the variation of R along the depth. The last column shows three vertical profiles of (i) Hydrolight derived (direct) R ($R_{HL\text{-}direct}$) (represented in green), (ii) Hydrolight R calculated form the Hydrolight outputs $E_u(\lambda,z)$, $E_d(\lambda,z)$, $K_u(\lambda,z)$, and $K_d(\lambda,z)$ ($R_{HL\text{-}AOP}$) (represented in blue), and (iii) R calculated from the present model (R_{model}). Figure 4(a) shows *Chl* maxima at the surface and decreases rapidly at 3-5 m and then increases at depths greater than 7m. The turbidity also closely follows this trend with an increase and a decrease in the top and bottom layers. A similar trend is replicated in the IOP profiles of *a*, *c* and b_b. The K_u and K_d profiles are the function of IOPs following a similar trend but with some additional effects of the light field available at respective depths. It becomes obvious that all the $R(\lambda,z)$ profiles show the variation following the trend of the IOP profiles with a decrease at 3-5 m and an increase at surface and bottom depths. It is also observed that the Hydrolight derived direct R ($R_{HL\text{-}direct}$), smoothly varies according to the IOP profile but fails to account for the variation component associated the *f* factor at that particular depth. However, the other two R ($R_{HL\text{-}AOP}$ and R_{model}) profiles capture the depth-wise variations accurately; particularly the increase in attenuation at 3-4m is accounted directly on K_u and the subsequent variations are produced in R. It means that the $K_u(\lambda,z)$ and $K_d(\lambda,z)$ have a significant role in influencing the R variation throughout the water column. The fluctuations of R due to the roughened sea state caused by wind are generally restricted to the upper column of the ocean. The three cases shown for three different stations were simulated for zero wind speed. Assuming the wind speed zero avoids the risk of greater (than the actual) downwelling radiances entering the sensor, and thus it is made sure that $K_u(\lambda,z)$ and $K_d(\lambda,z)$ do not contain the unwanted lighting effects other than those influenced by the water column properties. $K_u(\lambda,z)$ and $K_d(\lambda,z)$ as defined in Eq. 10 (as an AOP) can only determine the actual variations of R in the water column. As an IOP or quasi IOP, they would result in the homogeneous behavior of $R(\lambda,z)$ throughout the water column (thus appropriate to predict its variations in the water column). The increase/decrease behavior of R has been discussed in Tables 4, 5, 6 of Dev and Shanmugam (2014b). Figure 4(b) shows another example of increasing and decreasing IOPs and AOPs. In this case, *Chl* decreases toward the depth with slight fluctuations, while turbidity shows well pronounced features - a dip around 5 to 8 m and an increase at depth > 8m because of the presence of considerable amount of inorganic content in the bottom layer. The effects of IOPs and AOPs (K_u and K_d) give rise to the corresponding variations in R – i.e., a decrease at the intermediate layer and an increase at the bottom layer. Note that the $R_{HL\text{-}AOP}$ and R_{model} profiles are better consistent with those of the IOP profiles while the $R_{HL\text{-}direct}$ profile slightly deviates from the IOP profiles due to the missing component. In Fig. 4(c), the IOPs (and both chlorophyll and turbidity) continue to increase toward the depth and the same trend is reflected in AOPs (K_u, K_d) as well. K_u seems to be low when compared to K_d throughout the water column, giving rise to the enhanced $R(\lambda,z)$. Here the $R_{HL\text{-}direct}$ profile is nearly similar to the $R_{HL\text{-}AOP}$ and R_{model} profiles because of the relatively less effect of chlorophyll absorption and more influence of suspended sediment attenuation and backscattering with the increasing depth. These results suggest that the depth-wise R variations

can be predictable if $R(0^-,\lambda)$, $K_u(\lambda,z)$ and $K_d(\lambda,z)$ values are calculated correctly. The deduction of the $R(\lambda,z)$ is analytically correct and it is in line with the theory.

11. Figure 4: Which site with what IOPs is shown? Could you include the vertical distribution of IOPs used for the model! What are the related cases in Figure 3? It would be in addition helpful if you could include the percent relative difference of model vs. in situ data. The differences seem to be larger than normally considered as "generally good" (page 1902, 24), see e.g.: Zibordi, G., Donlon, C. J., & Parr, A. C. (2014). Optical Radiometry for Ocean Climate Measurements (Vol. 47). Academic Press. Mean but also highest values should be reported for all water types and carefully discussed.

The answers related to this section cover the answers of the previous section and it has been included in the revised manuscript. The new figure of depth profiles are shown below.

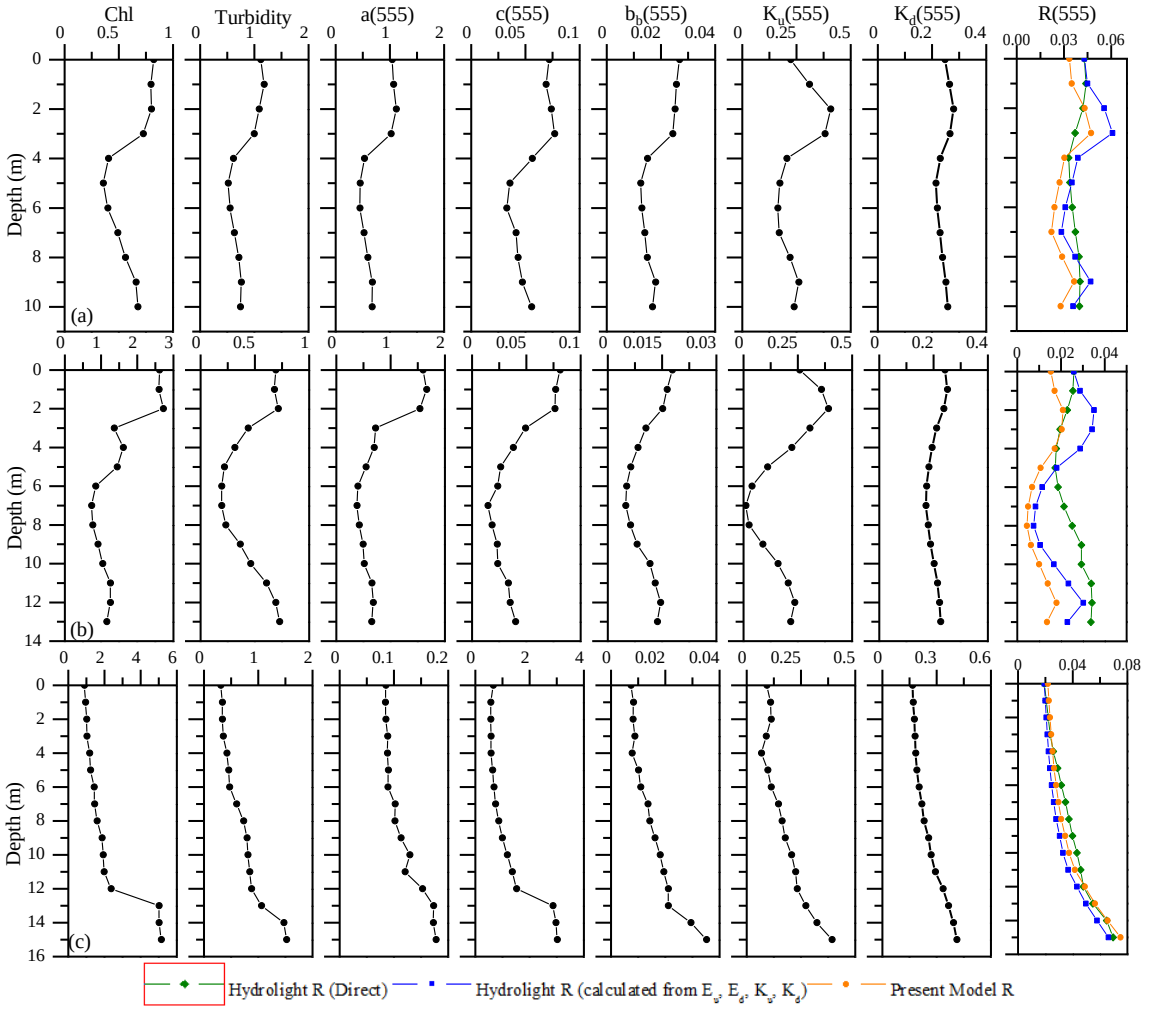

Figure 4. Vertical profiles of the *Chl*, *turbidity* and IOPs (total $a(555,z)$, $c(555,z)$, $b_b(555,z)$) for three different stations (considered as input for Hydrolight simulations) and the corresponding output profiles $K_u(555,z)$, $K_d(555,z)$ and $R(555,z)$. Last column represents Hydrolight direct R,

$R_{HL\text{-}direct}$ (Green line), Hydrolight R calculated from E_u, E_d, K_u and K_d, $R_{HL\text{-}AOP}$ (blue line) and the present model, R_{model} (orange line).

12. The model accuracy should be shown in detail for all water types. It would be desirable to see, where the model fits best and where other models, e.g. optimized for the open ocean, are able to keep up (e.g. similar to Dev, P. J. and Shanmugam, P.: New model for subsurface irradiance reflectance in clear and turbid waters, Opt. Express, 22, 9548–9566, 2014b).

The following text and the Table 3 has been added to the revised manuscript. The same is described under the Comment No: 5.

Comparing with the existing models, it should be noted that the existing models are designed with certain assumptions to predict R in case 1 waters or coastal (case 2) waters. For instance, a model that is originally developed for clear oceanic case 1 waters (Gordon et al., 1975; Morel and Prieur, 1977, Kirk, 1984) gives biased reflectance values in turbid coastal and productive water types. A model of case 2 waters (Albert and Mobley, 2003) is restricted to case 2 waters (Dev and Shanmugam, 2014b). Thus, it is more appropriate to compare the results of this study with our previous model since both the models are designed for both marine and inland waters. Figure 5(a)-(d) shows the scatter plots comparing the model R (from the model of Dev and Shanmugam (2014b) and this study) with *in-situ* R for all the water types, where the blue dots represent the previous model (Dev and Shanmugam, 2014b, denoted as *DS* in Table 3) and the orange dots represent the present model (denoted as *PM* in Table 3) for the key wavelengths 412, 443, 488, 531, 555, 650, 685, 715nm. In Fig. 5(a), results from both the models are nearly identical although the previous model slightly performs better (relative error 18.8%) than the present model (relative error 21.3%). These differences are noticeable in the range below 0.001 where the instrument noise could cause errors in clear oceanic waters when the reflectance values are almost zero in the NIR. In type II relatively clear waters, results from the present model start improving upon those of the previous model (Figure 5(b)), with the relative error of 18.2% for the present model and 15.3% for the previous model. The present model gives better results for the moderately turbid type III waters than the previous model (see the orange dots falling on the 1:1 line in Figure 5(c)). The relative error percentage of the present model is 10.5% when compared to 12.8% for the previous model. In Type IV sediment dominated turbid waters (Figure 5(d)), the present model yields the error percentage of <6% whereas the previous model yields around 21.3%. In the turbid productive type V waters, results from the present model are closer to the *in-situ* data (Figure 5(e)), thereby yielding the relative percentage error of less than 9% over 48% for the previous model. These results suggest that the model is well suited for optically complex coastal and inland waters with high organic and inorganic contents. These validation results clearly emphasize the importance of the present model for predicting R in a wide variety of waters without involving the spectral constants with the previous model. The additional parameters with the present model increase its potential and wider applicability.

Table 3. Relative differences between the model *R* from the previous work of [a]Dev and Shanmugam, 2014b (DS) and this study (present model - PM) and the in-situ *R* for the five water types.

		412	448	488	531	555	670	685	710	*average*
Type I	*PM*	0.277	0.081	0.113	0.242	0.274	0.242	0.033	0.445	0.213
	DS[a]	0.035	0.127	0.009	0.139	0.137	0.13	0.315	0.52	0.188
Type II	*PM*	0.215	0.239	0.17	0.181	0.171	0.191	0.266	0.021	0.182
	DS[a]	0.085	0.083	0.139	0.139	0.157	0.172	0.169	0.28	0.153
Type III	*PM*	0.23	0.16	0.072	0.028	0.011	0.028	0.163	0.145	0.105
	DS[a]	0.044	0.087	0.114	0.108	0.111	0.164	0.153	0.243	0.128
Type IV	*PM*	0.127	0.011	0.038	0.009	0.006	0.113	0.13	0.008	0.055
	DS[a]	0.178	0.197	0.177	0.2	0.196	0.22	0.254	0.279	0.213
Type V	*PM*	0.167	0.09	0.017	0.071	0.051	0.067	0.201	0.035	0.087
	DS[a]	0.125	0.368	0.542	0.312	0.619	0.674	0.619	0.639	0.487

13. Table 1: Is the table related to Figure 4? Could you provide percent relative differences too? It seems to be better to distinguish water types too.

The answers to this comment are described along with Comment no: 12 & 5. The Table 3 is provided to show the relative differences.

14. Figure 3: Could you provide further information in a table: a, c, bb, Chl, TSM, theta_s, and turbidity!

A table (table 1) is provided to show the optical properties range corresponding to Figure 3.

Table 1. Information regarding the optical properties and illumination conditions for those samples presented in Fig. 3.

Water Type	*Figure 3*	*a*(412) (m^{-1})	b_b(412) (m^{-1})	*Chl* (mg m^{-3})	*Turbidity* (NTU)	*Solar zenith angle* (deg)
Type I	a_1	0.129	0.0154	0.2	0.59	41.15
	a_2	0.132	0.016	0.23	0.6	25.52
Type II	b_1	0.385	0.0481	1.99	2.03	33.59
	b_2	0.493	0.0325	1.68	1.43	39.47
Type III	c_1	1.234	0.0383	17.72	1.86	42.38
	c_2	1.183	0.0471	16	2.23	53.8

Type IV	d_1	0.928	0.232	1.25	8.66	19.39
	d_2	0.56	0.1467	1.09	5.64	31.92
Type V	e_1	8.1	0.29	49.28	7.66	20.94
	e_2	6.56	0.24	44.64	7.79	54.91